Three-Dimensional EXIT Chart Analysis of Iterative Detection Aided Coded Modulation Schemes

R. Y. S. Tee, S. X. Ng and [1]L. Hanzo

School of ECS, University of Southampton, SO17 1BJ, UK.
Tel: +44-23-8059 3125, Fax: +44-23-8059 4508
Email: [1]lh@ecs.soton.ac.uk, http://www-mobile.ecs.soton.ac.uk

Abstract – **The iterative convergence of iteratively detected coded modulation schemes having different block lengths, decoding complexity and an unequal error protection capability is studied, when communicating over AWGN channels using 8PSK modulation. More specifically, the coded modulation schemes investigated include Multilevel Coding (MLC), Trellis Coded Modulation (TCM), Turbo Trellis Coded Modulation (TTCM), Bit-Interleaved Coded Modulation (BICM) as well as Bit-Interleaved Coded Modulation employing Iterative Decoding (BICM-ID). A novel three dimensional EXIT chart was introduced for studying the iterative convergence behaviour of the Multistage Decoding (MSD) scheme used in MLC.**

1. INTRODUCTION

The philosophy of coded modulation was proposed by Imai [1] in his pioneering work on Multilevel Coding (MLC) and by Ungerböck [2] in the context of Trellis Coded Modulation (TCM). MLC was originally designed for protecting each of the modulated bits using different component codes. It offers a flexible-rate code design philosophy and the attractive capability of providing unequal error protection. Classic channel capacity rules based on mutual information have formed the basis of designing the component codes' coding rates [3]. Multistage Decoding (MSD) has been widely used for the decoding of MLCs as the benefit of their reduced decoding complexity, while Parallel Independent Decoding (PID) has been proposed for the sake of reducing the associated decoding delay [4].

Trellis Coded Modulation (TCM) [2] was proposed based on the joint design of modulation and coding in order to maximize the Free Euclidean Distance (FED) when communicating over Additive White Gaussian Noise (AWGN) channels. TCM uses Ungerböck's Set Partitioning (SP) principle as its mapping strategy, which imposes a low decoding complexity. Turbo Trellis Coded Modulation (TTCM) [5] employs the well-established structure of Turbo codes [6] using TCM as its component codes. With the parallel concatenated turbo encoding structure in mind, the upper TCM component encoder processes the original information bits, while the lower TCM component encoder encodes an interleaved version of the upper one.

Zehavi further advanced the state-of-the-art by proposing Bit-Interleaved Coded Modulation (BICM) [7], where independent bit interleavers are used in conjunction with Gray Mapping for increasing the achievable time-diversity order and consequently to enhance the Effective Code Length L, especially in a Rayleigh fading environment. However, this is achieved at the expense of a reduced minimum Euclidean distance, which inevitably results in a reduced performance for transmission over AWGN channels. Bit Interleaved Coded Modulation assisted by Iterative Decoding (BICM-ID) [8] using a SP based mapping strategy was designed to improve the minimum Euclidean distance and to achieve an iteration gain in comparison to non-iterative BICM. The specific mapping of the bits to the symbols used in BICM-ID schemes determines much of the attainable performance gain and hence it has to be optimized.

In this paper, we comparatively study various coded modulation schemes. We invoke a novel 3D EXIT chart for characterizing the iterative MSD behaviour of MLC system compared to both BICM-ID and to TTCM schemes. The rest of the paper is organized as follows. In Section 2 we describe the system structure used. Our simulation results characterizing the different schemes are detailed in Section 3. In Section 4 we invoke EXIT charts in our convergence study, while our conclusions are presented in Section 5.

2. SYSTEM OVERVIEW

In our studied system, random information bits u are generated as our source data before being fed into the encoders. The bits v of the coded sequence are then appropriately interleaved and mapped to the 8PSK constellation points using the mapping function of $\mu(v)$. The channel imposes the AWGN n, where the complex AWGN-valued noise variables are represented by $n = n_I + jn_Q$, which have a variance and double sided noise power spectral density obeying $\sigma^2 = \sigma_I^2 = \sigma_Q^2 = N_0/2$.

At the receiver, the demapper converts the received signals to logarithmetic domain probabilities. These probabilities are then deinterleaved and fed into the appropriate bit or symbol-based log MAP decoders [6]. The log-domain branch metrics of the symbol-based MAP decoders [6] are computed based on the Gaussian PDF of

$$p(y_k|x_k) = \frac{1}{\sqrt{2\pi}\sigma_n} e^{-\frac{|y_k - x_k|^2}{2\sigma_n^2}}. \quad (1)$$

Both MSD [3] and PID [3] may be used for MLC decoding, where the N en(de)coders convey a total of N modulated bits. In MSD each *extrinsic* information value of protection level i, for $i \in \{0, 1, ..., N-1\}$ is fed back to the demapper, before being used by the decoder of protection level $(i+1)$. By contrast, in PID of MLC [3], all N decoders will carry out their decoding operation at the same time, before utilizing the *extrinsic* information in the next iteration. When encoding m number of data bits, the coding rate for TCM, BICM and BICM-ID becomes $R = \frac{m}{m+1}$ for a 2^{m+1}-ary modulated signal constellation. When the number of uncoded bits in TCM is $\overline{m} < m$, we have $2^{\overline{m}}$ parallel transition branches in the trellis, which results in a reduced decoding complexity [2]. In the context of MLC, the coding rate of the amalgamated scheme would be $R = R_0 + R_1 + ... + R_{N-1}$, when assuming N levels of potentially different-rate encoding. The coding rate of each component code of the MLC scheme to approach the channel capacity

The financial support of the EPSRC, UK and that of the European Union under the auspices of the Phoenix and Newcom projects is gratefully acknowledged.

Mapping Type	Mapping Indices to Corresponding Signal Points ($\cos 2\pi i/M$, $\sin 2\pi i/M$) for $i \in$ 0 1 2 3 4 5 6 7
Gray	0 1 3 2 6 7 5 4
SP	0 1 2 3 4 5 6 7
BP	7 3 6 2 4 0 5 1
MP	0 2 1 7 4 6 5 3

Table 1: Different bit to symbol Mapping Strategies : Gray, Set Partitioning (SP), Block Partitioning (BP) and Mixed Partitioning (MP) [3], where M is the number of constellation points.

may be determined with the aid of the capacity design rules of [3]. The chain rule of mutual information exchange in the context of our 8PSK schemes is formulated as $I(Y;A) = I(Y;X^0,X^1,X^2) = I(Y;X^0) + I(Y;X^1|X^0) + I(Y;X^2|X^0,X^1)$, where A is the random input symbol, X is the modulated symbol and Y is the received channel-contaminated symbol. Convolutional codes are used as component codes in all of the TCM, TTCM, BICM, BICM-ID and MLC schemes. These convolutional codes are punctured, when requiring high coding rates. For the sake of achieving the best possible performance, a range of different bit to symbol mapping strategies are employed in our coded modulation schemes. Specifically, Gray Mapping, Set Partitioning (SP), Block Partitioning (BP) and Mixed Partitioning (MP) [3] are used, which map the natural coded bits to the different modulated constellation points, as shown in Table 1.

3. SIMULATION RESULTS

In this section we present simulation results for the previously mentioned range of different coded modulation schemes. The effective throughput of the system is $\log_2(M)R$, when using an M-ary modulation constellation and an overall coding rate of R. The effective throughput is chosen ere as 2 Bits Per Symbol (BPS) with 8PSK modulation. The component codes are punctured convolutional codes of coding rate $R_0 = 1/3, R_1 = 3/4, R_2 = 11/12$ [4]. Due to the specific coding rates that are readily available for convolutional codes, we do not follow the exact capacity rules proposed in [3] for adjusting the MLC scheme's coding rate.

Coded modulation schemes exhibit an implementational complexity, which is exponentially proportional to both the number of trellis decoding states and the number of iterations. Since the number of trellis states is 2^K, where K is the memory of the codes, both TCM and BICM have a complexity, which is proportional to $\nu = 2^K$. TTCM invokes two TCM component codes and n decoding iterations, hence its complexity is proportional to $\nu = 2.n.2^K$. BICM-ID feeds its $extrinsic$ information from the decoder to the demodulator during each decoding iteration. The complexity of the demapper may be assumed to be insignificant. Hence BICM-ID exhibits a complexity, which is proportional to $\nu = n.2^M$. By contrast, MLC has i component codes with each of the component codes having a memory of K_i. Hence, its complexity at n iterations, when using MSD is commensurate with the sum of the individual decoder's complexity, which is expressed as $\nu = n.\sum_{i=0}^{i=N-1} 2^{K_i}$.

Figure 1 shows the beneficial effect of increasing the decoding complexity on the attainable BER performance of the various coded modulation schemes. All schemes have the same effective throughput of 2 BPS. Explicitly, 32-state MLC, 32-state BICM, 32-state TCM, 2x16-state TTCM and 32-state BICM-ID exhibit a similar complexity. Observe in Figure 1 that non-iterative TCM outperforms all the

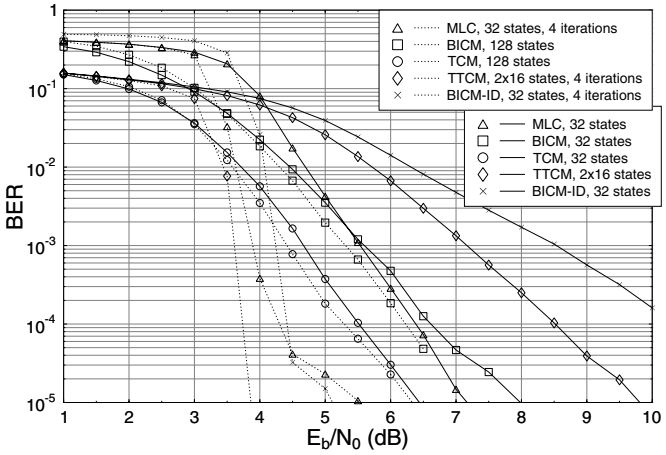

Figure 1: BER performance of 8PSK modulated MLC, TCM, TTCM, BICM and BICM-ID at a range of different complexities, for transmission over an AWGN channel using an interleaver block length of 1800 symbols.

other iterative schemes, which require several iterations to perform well. At BER = 10^{-4} TCM has an approximately 1dB coding advantage over both MLC as well as BICM, and a gain in excess of 3dB and 4dB, when compared to the corresponding TTCM and BICM-ID schemes, respectively. Without iterations, TTCM using punctured component codes does not benefit from sufficient $extrinsic$ information exchange. Similarly, BICM-ID which was derived for fading channels using SP but no iteration has a poor Hamming distance. Still referring to Figure 1, we then increased the complexity of the various coded modulation schemes both by invoking a higher memory length and by increasing the number of iterations. Observe that TTCM outperforms the other coded modulation arrangements, closely followed by MLC and BICM-ID, which have quite similar performances, requiring an E_b/N_0 around 4.4dB for achieving a BER of 10^{-4}. Increasing the memory length of TCM and BICM, the required E_b/N_0 becomes 5.3dB and 6.2dB, respectively. Hence, increasing the memory length of TCM and BICM from K=5 to K=7 and hence quadrupling their complexity improves the performance by less than 0.5dB, while the iterative TTCM, MLC and BICM-ID schemes exhibit a significant E_b/N_0 improvement of up to 5dB upon quadrupling their complexity, which renders the latter iterative schemes more attractive.

Figure 2 illustrates the effect of employing different interleaver block lengths by the various coded modulation schemes. More specifically, the block lengths of 180 and 1800 symbols are compared. Increasing the interleaver block length improves the attainable performance, especially for the iterative schemes of MLC, BICM-ID and TTCM. Observe in Figure 2 that BICM-ID has a high sensitivity to the interleaver's block length and at BER = 10^{-4} it exhibits an approximately 1.5dB gain over the similar-complexity non-iterative BICM scheme having 128 trellis states. As seen in Figure 2, MLC shows a 1.35dB increase in coding gain at BER = 10^{-4}, as a benefit of using N encoders, where each encoder requires a longer interleaver, when the input data is divided into a number of different-protection parallel streams. TCM and BICM obtain an E_b/N_0 improvement of less than 1.5dB at BER = 10^{-4} and hence they are outperformed by the iterative schemes, especially by TTCM, as evidenced by Figure 2.

Providing Unequal Error Protection (UEP) is important in the context of speech and video transmission. Figure 3 illustrates the fact that MLC is the most flexible scheme in terms of providing UEP among the coded modulation schemes studied, when combined with

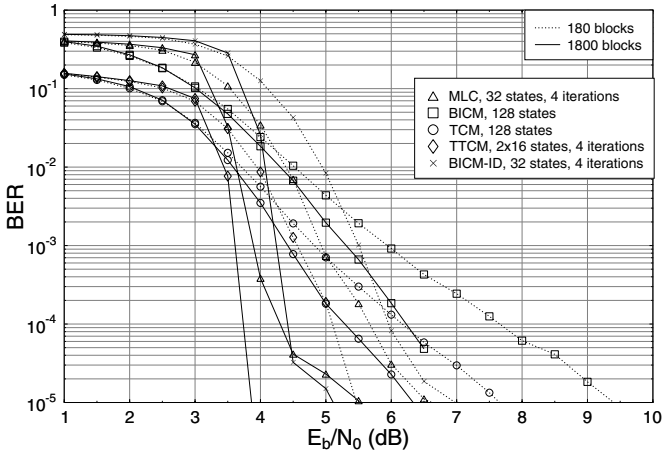

Figure 2: BER performance of 8PSK modulated MLC, TCM, TTCM, BICM and BICM-ID using different interleaver block lengths for transmission over AWGN channels at a given fixed complexity associated with a total of 128 trellis states.

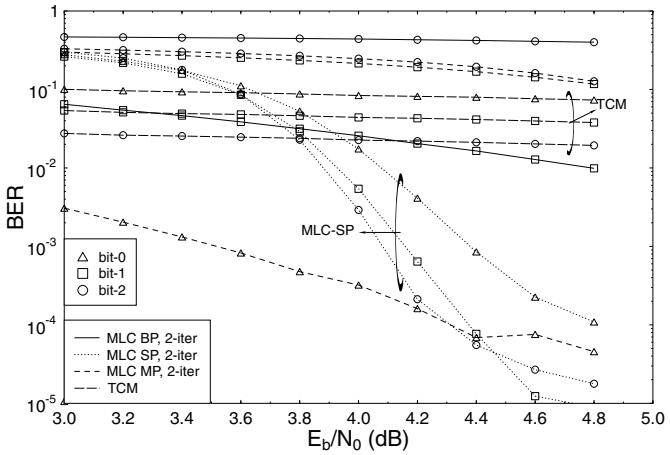

Figure 3: BER versus E_b/N_0 for the three different-integrity subchannels in MLC using SP, BP, MP mapping, as well as TCM assisted by two turbo iterations.

an appropriate choice of encoded bits to modulated symbol constellation mapping. To elaborate a little further, all schemes in this figure have three input data bits that have to be protected. The individual decoded bits of both BICM-ID and TCM exhibit a similar BER performance, i.e. they have no UEP capability, as stated above. Similarly, the SP based mapping of MLCs does not provide the required UEP either, which is a consequence of the fact that the stronger code is applied to the specific phasor constellation bits, which are separated by a small Euclidean distance, while the weaker codes at the higher protection levels of the MLC scheme are supported by a large Euclidean distance. The MLC scheme using BP has an equal Euclidean distance for all of its three different bits. Note that bit 0 of the BP-based MLC scheme exhibits a BER below 10^{-5} and thus its BER curve is not shown in the figure, while bit 2 has a clearly inadequate BER. The MP scheme has its bit 0 strongly protected, while both bit 1 and bit 2 exhibit a similarly inadequate BER performance.

4. EXIT CHART ANALYSIS

Extrinsic Information Transfer (EXIT) charts [9] constitute a useful tool in the design of iterative schemes, since the characteristics of the constituent components can be visualized based on their exchange of mutual information.

In our MLC schemes, the output of each convolutional component code is bit interleaved for the sake of providing an independent source of time diversity, since as a benefit of interleaving, the corresponding bit streams become fairly uncorrelated. The output LLRs of the decoders exhibit a Gaussian-like distribution [9]. Similarly, the input $a\ priori$ information A of each component decoder is modeled by an independent Gaussian distribution. The mutual information of the $a\ priori$ LLRs of the decoder is given by [9]

$$I_A(\sigma_A) = 1 - \int_{-\infty}^{\infty} \frac{e^{-((y-\sigma_A^2/2)^2/\sigma_A^2)}}{\sqrt{2\pi}\sigma_A} \log_2[1+e^{-y}]\mathrm{d}y, \qquad (2)$$

where σ_A^2 is the variance of A. Given a sufficiently high number of received signal samples N and the $a\ priori$ LLRs L_n of a sequence of n bits, the mutual information of the decoder's extrinsic LLRs can be expressed as [10]

$$I_E = 1 - E\{\log_2(1+e^{-L})\} \approx 1 - \frac{1}{N}\sum_{n=1}^{N} \log_2(1+e^{-x_n \cdot L_n}), \quad (3)$$

where x_n represents a sequence of n transmitted bits, which constitute a subset of the total of N samples.

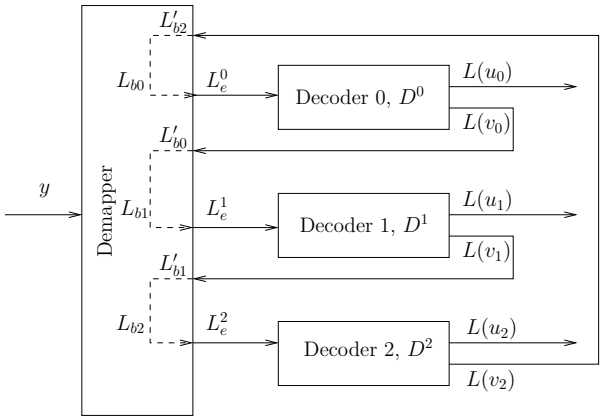

Figure 4: MSD decoder of the 8PSK modulated MLC scheme with channel information y. The notations $L(u_i)$ and $L(v_i)$ represent the output LLRs of the three decoders for both the information bits and the encoded bits. The subscript i represents the bit index in $b0$, $b1$ and $b2$. Furthermore, L_{bi} denotes the associated information bits' LLRs for the corresponding decoder D^i, which is further augmented in Figure 5, while L'_{bi} denotes the $a\ priori$ LLRs forwarded by the $other$ decoders D^i to the input of the inner demapper. L^i_e denotes the $extrinsic$ LLRs provided by the demapper.

Figure 4 illustrates a three-level UEP MSD MLC design using 8PSK modulation and three decoders, namely D^0, D^1 and D^2 for bit 0 ($b0$), bit 1 ($b1$) and bit 2 ($b2$) respectively. In Figure 5, we show the general structure of EXIT chart generation for the MSD of Figure 4. Note that L_A represents the LLRs of the information bits of the relevant decoder, while $L^i_{A(o)}$ denotes the LLRs of the $other$ decoders' information bits. Considering the decoder at protection $level$ 0 and referring to the schematic of Figure 5, the associated information bit is $b0$, while the corresponding information bits of the other decoders are

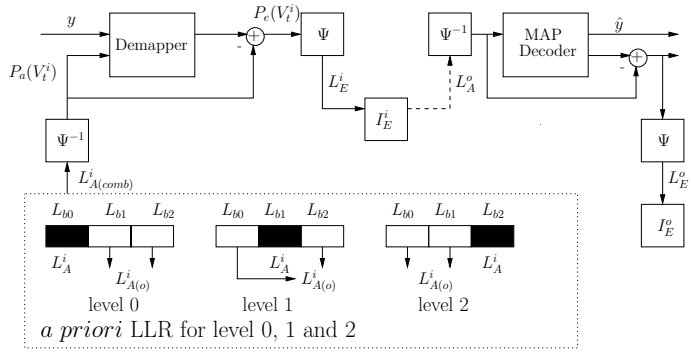

Figure 5: General structure of EXIT chart generation for the MSD of 3-level MLC when using 8PSK and three en(de)coders. L_b^a represents the LLR values, where the superscript a denotes the inner (i) or outer (o) codes, while the subscript b denotes the input *a priori* (A) or output *extrinsic* (E) information. L_{b0}, L_{b1} and L_{b2} are independent Gaussian distributed LLR generated for bits 0, 1 and 2 respectively. Furthermore, Ψ and Ψ^{-1} denote the LLR-to-symbol probability and symbol probability-to-LLR conversion. The arrow drawn in dash line represents the *extrinsic* LLR demapper output, which becomes the LLR input of the decoder after demapping. The filled black box represents the *a priori* LLR of the associated information bit, while the hollow box denotes the *a priori* LLR of the bits of the *other* decoders. Finally, I_E^i and I_E^o denote the mutual information used for plotting the EXIT chart.

$b1$ and $b2$, respectively. Hence L_A^i, which is the LLR associated with the black box in the figure, is generated from L_{b0}. The *a priori* LLRs generated by the *other* decoders are L_{b1} and L_{b2}, as indicated by the hollow boxes in Figure 5, are then computed along with their individual average values for the sake of obtaining the combined *a priori* LLR of $L_{A(o)}^i$ as the input soft bit value for the iterative demapper. Similar operations are carried out at the *level* 1 and 2 decoders, each having the corresponding information bit represented by the black box at different position in Figure 5. The demapper of the MLC decoder is treated similarly to the demodulator of the iterative BICM-ID [11] scheme. When the *a priori* probability P_a is different from 0.5, the extrinsic probability of the MLC demapper is given by [11]

$$P_e(v_t^i = b) = \sum_{v_t \in \chi(i,b)} \left(P(y_t|x_t) \prod_{j \neq i} P_a(v_t^j = v^j(x_t)) \right). \quad (4)$$

For 8PSK modulation, the bit index is $i = 0, 1, 2$, where we have $v^i = b$, $b \in \{0, 1\}$, and following the notation of [11], the subset of modulated signals is denoted by $\chi(i, b) = \{\mu(v^0, v^1, v^2) | v^i = b; v^j \in 0, 1, j \neq i\}$. The mapping function $\mu(.)$ of the different mapping schemes, used in our design study was illustrated in Table 1. For an AWGN channel, $P(y_t|x_t)$ is given by Equation 1. Since we have $j \neq i$, which excludes the own intrinsic information of each bit, the output LLR is only affected by the *extrinsic* information of the *other* decoders. Let us now investigate the decoding convergence of the schemes studied using a three-dimensional (3D) EXIT chart with reference to Figure 5 in the context of three different en(de)coders employing SP based labeling. To expound a little further, the reason for requiring a 3D EXIT chart in the context of our 8PSK based MLC scheme is, because when employing MSD there is an iterative information exchange amongst the three separate MLC decoders of the different protection levels, rather than between only two constituent decoders, as in the case of conventional EXIT charts. The results of our 3D EXIT chart analysis are shown in Figure 6. At each level of the MLC decoding scheme, the demapper constitutes the inner decoder, while the outer decoders are the corresponding MAP decoders.

In Figure 6, I_A^i/I_E^i and I_A^o/I_E^o denote the mutual information of the inner and outer codes, respectively. Furthermore, $I_{A(o)}^i$ in Figure 6 represents the mutual information at the demapper's input generated from the *a priori* knowledge provided by the *other* decoders, where the superscript i represents the *inner* code, while the subscript $A(o)$ represents the *a priori* knowledge gleaned from the *other* decoders. As seen in Equation 4, the *extrinsic* probability information exploited by the MLC demapper is only affected by the information bits provided by the *other* decoders, hence I_E of the demapper changes only as a function of $I_{A(o)}^i$, as seen in Figure 6. As observed in Figure 5, the mutual information is exchanged between the inner demapper by passing I_E^i to the outer MAP decoder, which iteratively exchanges I_E^o with the inner demapper. In the 8PSK based MLC scheme, we have three different-integrity decoding levels ($b0$, $b1$, $b2$) and each level is represented in one of the three 3D EXIT charts shown in Figures 6(a), 6(b) and 6(c), respectively. In Figure 6, the EXIT plane marked with triangles is computed based on the inner demapper's output *extrinsic* information I_E^i at a given *a priori* input I_A^i and $I_{A(o)}^i$, characterizing its *extrinsic* probability P_e forwarded to the outer MAP decoders. By contrast, the EXIT plane of Figure 6, which is represented by the mesh of rectangles was obtained based on the MAP decoder's *extrinsic* output I_E^o at a given demapper extrinsic information I_E^i.

Commencing from decoder 0 having only the channel's output information, but no *a priori* LLR from the *other* decoders, the I_E^i trajectory curve emanates from the central corner of the graph in Figure 6(a), with the x, y coordinate values equal to 0. When the *extrinsic* LLR L_e^i provided by the demapper output seen in Figure 4 is passed to D^0, the decoding trajectory moves in a direction parallel to the x axis at a certain I_E^o value, quantifying the *extrinsic* information contribution of the outer decoder D^0. The output *extrinsic* LLR $L(v_0)$ is then passed to the second-level demapper, where it becomes the *a priori* information L'_{b0}, as seen in Figure 4. Hence, at the second decoding level, the demapper benefits from both the channel LLRs and the *a priori* LLRs L'_{b0} provided by the first decoded level. We can therefore observe that $I_{A(o)}^i$ of level 1 in Figure 6(b) emerges from a positive value of the y axis. The iterative process evolves further then to the third decoder output at protection level 2, as shown in Figure 6(c). At the third decoder D^2 of Figure 4, the *extrinsic* LLRs $L(v_2)$ are fed back as the *a priori* information L'_{b2} to the decoder D^0 of the first level. At this stage, namely during the second iteration, we can observe from Figure 6(a) that the trajectory of $I_{A(o)}^i$ moves in parallel to the y axis as a benefit of the *a priori* knowledge L'_{b1} and L'_{b2} provided by the *other* decoders from protection level 1 and level 2 of the MLC scheme, and the output of the demapper 0 benefits from an iteration gain, where the decoding trajectory moves vertically along the z axis, between the two EXIT planes denoted by the mesh of triangles and rectangles, respectively, reaching a specific value of I_E^i. This is the *extrinsic* information gleaned during the second iteration in decoder 0. The same process continues, as the *a priori* information is forwarded from the first protection level towards the third protection level of the MLC scheme.

We observe in Figure 6, that the zig-zag shaped trajectory evolves within the 3D tunnel constituted by the inner demapper's and outer decoder's EXIT curves. The highest possible iteration gain would be reached, if the trajectory converged to the point Q (1,1,1). However, due to the deficient demapper characteristic, the decoding trajectory of Figure 6(a) fails to reach this point at protection level 0, since it is trapped between the EXIT planes. By contrast, the demapper characteristics reach better convergence both at protection level 1 and 2,

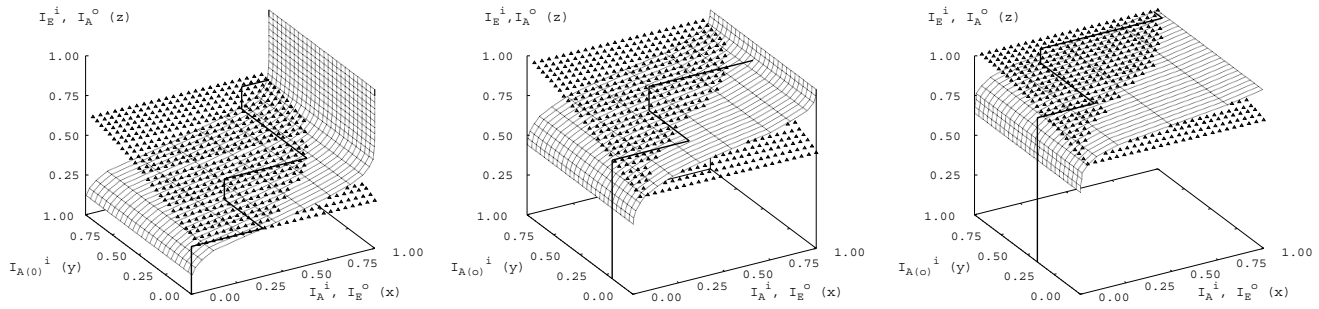

(a) Level 0 (b) Level 1 (c) Level 2

Figure 6: 3D EXIT Chart for Level 0, Level 1 and Level 2 of the MLC scheme at SNR = 4dB.

as seen in Figure 6(b) and 6(c) respectively, approaching the point Q (1,1,1) more closely. Hence, the iterative MLC scheme's performance is limited. Furthermore, note that the decoding trajectory fits closely, but not exactly into the EXIT chart's tunnel due to the fact that the MLC scheme's three encoded bits become slightly dependent on each other after the first iteration and therefore the corresponding LLRs do not obey a perfect Gaussian distribution. Nonetheless, the 3D EXIT chart provides an adequate prediction of the MLC scheme's iterative behaviour.

For the sake of comparison, Figure 7 shows the conventional two-dimensional EXIT chart of the BICM-ID and TTCM schemes studied in Figures 1 and 2. As observed, the EXIT chart tunnel of the BICM-ID scheme is relatively narrow and converges slowly to the P (1,1) point, requiring I=5 iterations to acquire its maximum iteration gain. By contrast, in the case of TTCM the tunnel is wider and steeper. When using I=3 iterations, the system approaches its best possible performance, even though it starts at a lower initial I_A value. We note furthermore that a narrow EXIT chart tunnel is indicative of operating close to channel capacity, possibly beyond the channel's cut-off rate, where further performance improvements are only achieveable at the cost of a high interleaver delay and high complexity, associated with a high number of iterations.

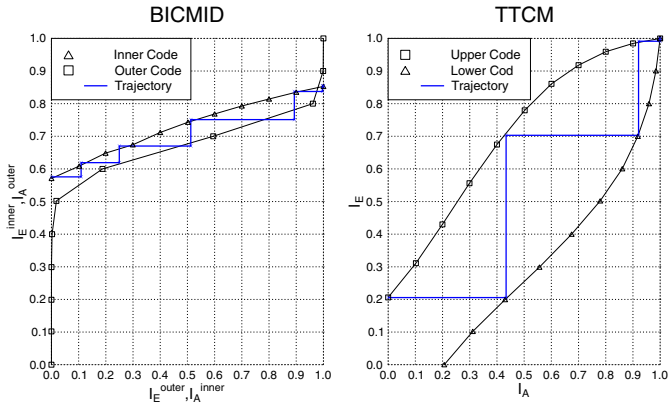

Figure 7: EXIT Charts for BICM-ID and TTCM at SNR = 4dB.

5. CONCLUSIONS

In conclusion, this paper provided a 3D EXIT chart based comparative study of a range of coded modulation schemes. TTCM was shown in Figure 1 and 2 to outperform the other schemes at a given implementational complexity associated with a total of 128 trellis states. Figure 1 demonstrated that even though the performance of TCM may become better than that of BICM upon increasing the complexity to 128 trellis states, TCM is outperformed by the iterative MLC and BICM-ID schemes, both of which exhibit a coding advantage close to 1dB. Of all coded modulation schemes considered, MLC has the ability to provide UEP and its average performance is close to that of the BICM-ID scheme. Our 3D EXIT chart of Figure 6, which was designed for MSD constitutes an efficient prediction of the joint iterative decoding performance of the inner demapper and outer decoder. An improved joint design of the demapper and decoder using non-binary precoders constitutes our future research.

6. REFERENCES

[1] H. Imai and S. Hirawaki, "A New Multilevel Coding Method Using Error Correcting Codes," *IEEE Transactions on Information Theory*, pp. 371–377, May 1977.

[2] G. Ungerböck, "Channel Coding with Multilevel/Phase Signals," *IEEE Transactions on Information Theory*, vol. 28, pp. 55–67, January 1982.

[3] U. Wachsmann, R. F. H. Fischer and J. B. Huber, "Multilevel Codes: Theoretical Concepts and Practical Design Rules," *IEEE Transaction on Information Theory*, vol. 45, pp. 1361–1391, July 1999.

[4] M. Isaka and H. Imai, "On the Iterative Decoding of Multilevel Codes," *IEEE Journal on Selected Areas in Comms*, vol. 19, pp. 935–943, May 2001.

[5] P. Robertson and T. Wörz, "Bandwidth-Efficient Turbo Trellis-Coded Modulation Using Punctured Component Codes," *IEEE Journal on Selected Areas in Communications*, vol. 16, pp. 206–218, February 1998.

[6] L. Hanzo, T. H. Liew and B. L. Yeap, *Turbo Coding, Turbo Equalisation and Space Time Coding for Transmission over Wireless channels*. New York, USA: John Wiley IEEE Press, 2002.

[7] E. Zehavi, "8-PSK Trellis Codes for a Rayleigh Fading Channel," *IEEE Transactions on Communications*, vol. 40, pp. 873–883, May 1992.

[8] X. Li and J. A. Ritcey, "Bit-Interleaved Coded Modulation with Iterative Decoding," *IEEE Communications Letters*, vol. 1, pp. 169–171, November 1997.

[9] S. ten Brink, "Convergence Behavior of Iteratively Decoded Parallel Concatenated Codes," *IEEE Transactions On Communications*, pp. 1727–1737, October 2001.

[10] J. Hagenauer, "The EXIT Chart - Introduction To Extrinsic Information Transfer In Iterative Processing," *Proceedings of 12th European Signal Processing Conference (EUSIPCO)*, pp. 1541–1548, September 2004.

[11] X. Li and J. A. Ritcey, "Bit-Interleaved Coded Modulation with Iterative Decoding Using Soft Feedback," *IEE Electronics Letters*, vol. 34, pp. 942–943, May 1998.